

# The study of nonstrange quark stars within a modified NJL model

Cheng-Ming Li<sup>1,\*</sup>, Shu-Yu Zuo<sup>2,†</sup>, Ya-Peng Zhao<sup>3,‡</sup>, Hui-Jun Mu<sup>1</sup>, and Yong-Feng Huang<sup>4,‡</sup>

<sup>1</sup> *School of Physics and Microelectronics, Zhengzhou University, Zhengzhou 450001, China*

<sup>2</sup> *College of Science, Henan University of Technology, Zhengzhou 450000, China*

<sup>3</sup> *School of Mathematics and Physics, Henan Urban Construction University, Pingdingshan 467036, China and*

<sup>4</sup> *School of Astronomy and Space Science, Nanjing University, Nanjing 210023, China*

In this work, a modified Nambu-Jona-Lasinio (NJL) model with proper-time regularization is employed to study the structure of nonstrange quark stars. The coupling constant of four-fermion interaction in the conventional NJL model is modified as  $G = G_1 + G_2 \langle \bar{\psi}\psi \rangle$  to highlight the feedback of quark propagator to gluon propagator. To study the dependence of the equation of state (EOS) on this modification as well as the vacuum pressure, we choose nine representative EOSs for comparison. It is found that a smaller  $G_1$  leads to a stiffer EOS, and a higher vacuum pressure (i.e., a smaller bag constant) yields a softer EOS at low energy density. It is further shown that the heaviest quark star under this modified NJL model satisfies not only the recent mass measurement of PSR J0740+6620, but also the radius constraints from X-ray timing observations. The corresponding tidal deformability is also in agreement with the observations of GW170817.

Key-words: nonstrange quark star, Nambu-Jona-Lasinio model, equation of state, proper-time regularization

PACS Numbers: 12.38.Lg, 25.75.Nq, 21.65.Mn

## I. INTRODUCTION

The structure of neutron stars and quark stars is largely determined by the equation of state (EOS) of dense matter. Given a particular EOS, the corresponding mass-radius ( $M$ - $R$ ) and mass-central energy density ( $M$ - $\epsilon_c$ ) relations can be obtained by solving the Tolman-Oppenheimer-Volkoff (TOV) equation. Since neutron stars and quark stars are composed of strongly interacting matter at high densities under a relatively low temperature, nonperturbative quantum chromodynamics (QCD) is deeply involved in exploring the EOS and structure of these compact stars. There are two critical features in QCD, i.e., color confinement and dynamical chiral symmetry breaking. At low chemical potentials, quarks are confined in hadrons under a low temperature. However, at high chemical potentials, quarks become deconfined. As a result, the observed highly compact pulsars could be quark stars rather than normal neutron stars.

In light of the hypothesis that strange quark matter might be the ground state of strongly interacting matter [1–4], many authors have extensively studied the characteristics of strange quark stars, either pure quark stars or hybrid neutron stars with a quark core [5–12]. Interestingly, a recent study [13] shows that stable quark matter might not be strange so that nonstrange quark stars can exist. Further studies have been carried out based on this viewpoint [14–18]. In Refs. [14, 15], a new self-consistent mean-field approximation is employed to study

the properties of nonstrange quark stars, such as the  $M$ - $R$  relation and the tidal deformability. Note that the difference between Ref. [14] and Ref. [15] is that the authors of Ref. [14] adopted the proper-time regularization, while a three-momentum cutoff regularization is used in Ref. [15]. A recent study [19] demonstrated that both the nonstrange and strange quark matter could be absolutely stable under the combination of the quark vector interaction and exchange interaction. Therefore, for two-flavor quark matter and three-flavor quark matter, which one is more stable is still an open question at present. In this study, we will investigate the properties of nonstrange quark stars in depth, providing useful constraints the EOS of nonstrange quark matter with recent astronomical observations.

Since Jocelyn Bell and Antony Hewish discovered PSR B1919+21 in 1967, a large number of pulsar mass measurements have been obtained till now. Among these measurements, PSR J0348+0432 and PSR J0740+6620 are two special examples characterized by their large masses, i.e.,  $2.01 \pm 0.04 M_\odot$  (solar mass) [20] and  $2.14^{+0.10}_{-0.09} M_\odot$  [21], respectively. In recent years, the radii of a few pulsars were also encouragingly measured at unprecedented precision due to successful operation of the Neutron Star Interior Composition Explorer (NICER) [22–24]. For example, in Ref. [22], the radius of a typical  $1.44 M_\odot$  pulsar is found to be larger than 10.7 km. Additionally, the recently discovered gravitational wave (GW) event GW170817 has opened a new era of multi-messenger astronomy [25–40], and the LIGO-VIRGO collaboration provided useful constraints on the dimensionless tidal deformability ( $\Lambda$ ) of neutron stars through GW waveform observations during the inspiral phase of the binary neutron star (BNS) merger. For the star of low-spin priors, it is estimated

\* licm@zzu.edu.cn

† zhaoyapeng2013@hotmail.com

‡ hyf@nju.edu.cn

as  $\Lambda(1.4M_\odot) \leq 800$  [25], and the  $\Lambda_1 - \Lambda_2$  relation of GW170817 is also constrained by considering particular waveform models, such as the TaylorF2 waveform [41].

Lattice regularized QCD calculations are troubled by the famous “sign problem” at finite chemical potentials, making it difficult to perform calculations based on the first principles. As a result, we have to resort to some effective models to calculate the EOS of quark matter. Astronomical observations are then used to test these hypothetical EOSs. In general, the EOS should not be too soft since it will fail to produce the massive stars of  $\sim 2M_\odot$  as observed. At the same time, the EOS also should not be too stiff when the upper limit of the tidal deformability is considered, as hinted by the observational results of GW170817.

In this study we use a modified Nambu-Jona-Lasinio (NJL) model to study the structure of strange stars. Inspired by the operator product expansion (OPE) approach, the traditional constant coupling coefficient of the 2-flavor NJL model is modified as  $G = G_1 + G_2 \langle \bar{\psi}\psi \rangle$  with  $G_2 \langle \bar{\psi}\psi \rangle$  accounting for the feedback of the quark propagator to the gluon propagator (see for instance Ref. [7, 42–48]). The EOS of nonstrange quark matter derived in this framework will be used to study the properties of quark stars, especially the  $M - R$  relation and the tidal deformability.

Many studies have focused on the NJL model with t’ Hooft interaction [6, 19]. Although our gap equation in the SU(2) case looks similar to previous SU(3) studies which possesses a quadratic dependence on the quark condensate, we would like to point out that the reason is different here. In Ref. [6, 19], the t’ Hooft interaction term leads to the above quadratic dependence. But in this study, the modification of the coupling constant  $G$  is responsible for the effect.

This paper is organized as follows. In Section II, a brief introduction on the modified 2-flavor NJL model is presented, and nine representative EOSs for nonstrange quark matter are derived. In Section III, the tidal deformability and the  $M - R$ ,  $M - \epsilon_c$  relations are calculated for quark stars, and compared with astronomical observations. Finally, a brief summary and discussion is presented in Section IV.

## II. EOS OF NONSTRANGE QUARK MATTER

The NJL model is widely used as an effective model to describe cold dense quark matter in neutron stars and quark stars [49, 50]. The general form of the Lagrangian for the 2-flavor NJL model is:

$$\mathcal{L} = \bar{\psi}(i\not{\partial} - m)\psi + G[(\bar{\psi}\psi)^2 + (\bar{\psi}i\gamma^5\tau\psi)^2], \quad (1)$$

where  $m$  denotes the current quark mass, and  $G$  is the four-fermion coupling constant<sup>1</sup>. The interaction term  $G[(\bar{\psi}\psi)^2 + (\bar{\psi}i\gamma^5\tau\psi)^2]$  includes the scalar-scalar and pseudoscalar-isovector channels.

In general, the effective quark mass  $m_{\text{eff}}$  can be obtained by the self-consistent gap equation of

$$m_{\text{eff}} = m - 2G\langle \bar{\psi}\psi \rangle, \quad (2)$$

where  $\langle \bar{\psi}\psi \rangle$  is the quark condensate. At a zero temperature and zero chemical potential, it can be calculated as

$$\begin{aligned} \langle \bar{\psi}\psi \rangle &= - \int \frac{d^4p}{(2\pi)^4} \text{Tr}[iS(p^2)] \\ &= -N_c \int_{-\infty}^{+\infty} \frac{d^4p}{(2\pi)^4} \frac{8im_{\text{eff}}}{p^2 - m_{\text{eff}}^2}, \end{aligned} \quad (3)$$

where the trace “Tr” is evaluated in color, flavor, and Dirac spaces, and  $S(p^2) = \frac{1}{\not{p} - m_{\text{eff}}}$  represents the quark propagator.

To proceed, we need to convert our equations from the Minkowski space to the Euclidean space and employ some kinds of regularization. In this study, we adopt the proper-time regularization (PTR), a covariant regularization that has a “soft” cutoff to avoid the ultraviolet divergence when the momentum integration is to infinity. The formula of PTR is

$$\begin{aligned} \frac{1}{X^n} &= \frac{1}{(n-1)!} \int_0^\infty d\tau \tau^{n-1} e^{-\tau X} \\ &\xrightarrow{\text{UV cutoff}} \frac{1}{(n-1)!} \int_{\tau_{\text{UV}}}^\infty d\tau \tau^{n-1} e^{-\tau X}, \end{aligned} \quad (4)$$

where the integral limit  $\tau_{\text{UV}}$  is related to the ultraviolet cutoff  $\Lambda_{\text{UV}}$ :  $\tau_{\text{UV}} = \Lambda_{\text{UV}}^{-2}$ . Adopting the PTR regularization, Eq. (3) becomes

$$\begin{aligned} \langle \bar{\psi}\psi \rangle &= -N_c \int_{-\infty}^{+\infty} \frac{d^4p^E}{(2\pi)^4} \frac{8im_{\text{eff}}}{(p^E)^2 + m_{\text{eff}}^2} \\ &= -\frac{N_c}{(2\pi)^4} \int_{-\infty}^{+\infty} \int_{-\infty}^{+\infty} d^3\vec{p} dp_4 \frac{8m_{\text{eff}}}{p_4^2 + \vec{p}^2 + m_{\text{eff}}^2} \\ &= -\frac{6m_{\text{eff}}}{\pi^2} \int_0^{+\infty} dp \frac{p^2}{\sqrt{p^2 + m_{\text{eff}}^2}} \\ &= -\frac{6m_{\text{eff}}}{\pi^{\frac{2}{5}}} \int_{\tau_{\text{UV}}}^\infty \int_0^{+\infty} d\tau dp \tau^{-\frac{1}{2}} p^2 e^{-\tau(m_{\text{eff}}^2 + p^2)} \\ &= -\frac{6m_{\text{eff}}}{4\pi^2} \int_{\tau_{\text{UV}}}^\infty d\tau \frac{e^{-\tau m_{\text{eff}}^2}}{\tau^2}, \end{aligned} \quad (5)$$

where the superscript  $E$  means the parameter is measured in the Euclidean space.

According to the NJL theory, the coupling constant  $G$  represents the effective gluon propagator. Note that

<sup>1</sup> An exact isospin symmetry between u and d quark is adopted in this work so that  $m_u = m_d = m$ .

the quark and gluon propagators satisfy different Dyson-Schwinger (DS) equations, but they should couple with each other in view of QCD theory. As we know, quark propagators in the Nambu phase and Wigner phase are very different from each other [51–53], so the corresponding gluon propagators in these two phases should also be different. However, in the normal NJL model,  $G$  is simplified as a constant and remains the same in both the Nambu phase and the Wigner phase, which is obviously unreasonable. Additionally, simulations of lattice QCD have shown that the gluon propagator should vary with temperature, while its dependence on the chemical potential is more uncertain. In most NJL calculations, the effective gluon propagator  $G$  is usually assumed to be “static”, which thus does not depend on the temperature and chemical potential. It is obviously in contradiction with the requirements exerted on an effective gluon propagator.

The plane wave method in the QCD sum rule approach is used in Ref. [54]. It is argued that the full Green function (which is unknown) can be divided into two parts: the nonperturbative part and the perturbative part. The condensates are then expressed as various moments of the nonperturbative Green function. Therefore, the most general form of the “nonperturbative” gluon propagator is

$$D_{\mu\nu}^{\text{npert}} \equiv D_{\mu\nu}^{\text{full}} - D_{\mu\nu}^{\text{pert}} \equiv c_1 \langle \bar{\psi}\psi \rangle + c_2 \langle G^{\mu\nu} G_{\mu\nu} \rangle + \dots, \quad (6)$$

where  $\langle G^{\mu\nu} G_{\mu\nu} \rangle$  is the gluon condensate,  $c_1$  and  $c_2$  are coefficients that can be calculated with the QCD sum rule approach [55, 56], and the ellipsis refers to the contributions from other condensates (e.g., the mixed quark-gluon condensate).

Among all the condensates, the quark condensate has the lowest dimension, and a nonzero value of which, in the chiral limit, just signals the dynamical chiral symmetry breaking. Therefore, it is the elementary item and plays the most important role in the QCD sum rule approach. In this study, we will treat its contribution separately, while the contribution of other condensates is included in the perturbative part of the gluon propagator. In the framework of the NJL model, it is equivalent to a modification of

$$G \rightarrow G_1 + G_2 \langle \bar{\psi}\psi \rangle, \quad (7)$$

which is quite similar to the approach in Refs. [7, 42–48]. Under this modification, the coupling strength  $G$  will depend on both u and d quark condensates.  $G_2$  can be regarded as an effective coupling strength, reflecting the relative weight of the influence of the quark propagator and gluon propagator<sup>2</sup>.

TABLE I. Parameters adopted in this study.

$m$ [MeV]	$\Lambda_{\text{UV}}$ [MeV]	$m_{\text{eff}}$ [MeV]	$-\langle \bar{\psi}\psi \rangle^{\frac{1}{3}}$ [MeV]	$G$ [GeV <sup>-2</sup> ]	$G_1$ [GeV <sup>-2</sup> ]	$G_2$ [GeV <sup>-5</sup> ]
					1.935	-1.582
3.5	1324	180	353	2.005	2.005	0
					2.100	2.161

In this study, we will take three representative sets of  $(G_1, G_2)$  and then constrain the corresponding EOSs with astronomical observations (see Sec. III for more details). The current quark mass is taken as  $m = (m_u + m_d)/2 = 3.5$  MeV [57]. Similar to Ref. [49], we fix the parameters  $(\Lambda_{\text{UV}}, G)$  to reproduce the experimental data ( $f_\pi = 92$  MeV,  $m_\pi = 135$  MeV). The complete parameter sets adopted, including  $G_1$  and  $G_2$ , are presented in Table. I.

Here, we will also extend our calculations to zero temperature and finite chemical potential, which is equivalent to perform a transformation in the Euclidean space as [58]

$$p_4 \rightarrow p_4 + i\mu. \quad (8)$$

The quark condensate and number density can then be derived as

$$\begin{aligned} \langle \bar{\psi}\psi \rangle &= -N_c \int_{-\infty}^{+\infty} \frac{d^4 p}{(2\pi)^4} \frac{8m_{\text{eff}}}{(p_4 + i\mu)^2 + m_{\text{eff}}^2 + \vec{p}^2} \\ &= -\frac{6m_{\text{eff}}}{\pi^3} \int_0^{+\infty} dp \int_{-\infty}^{+\infty} dp_4 \frac{p^2}{(p_4 + i\mu)^2 + m_{\text{eff}}^2 + p^2} \\ &= \begin{cases} -\frac{6m_{\text{eff}}}{\pi^2} \int_{\sqrt{\mu^2 - m_{\text{eff}}^2}}^{+\infty} dp \frac{[1 - \text{Erf}(\sqrt{m_{\text{eff}}^2 + p^2} \sqrt{\tau_{\text{UV}}})] p^2}{\sqrt{m_{\text{eff}}^2 + p^2}}, & m_{\text{eff}} < \mu \\ \frac{3m_{\text{eff}}}{2\pi^2} \left[ -m_{\text{eff}}^2 \text{Ei}(-m_{\text{eff}}^2 \tau_{\text{UV}}) - \frac{e^{-m_{\text{eff}}^2 \tau_{\text{UV}}}}{\tau_{\text{UV}}} \right], & m_{\text{eff}} > \mu \end{cases} \end{aligned} \quad (9)$$

$$\begin{aligned} \rho_i(\mu) &= \langle \psi^\dagger \psi \rangle_i \\ &= -N_c \int \frac{d^4 p}{(2\pi)^4} \text{tr} [iS_i \gamma_0] \\ &= 2N_c \int \frac{d^3 p}{(2\pi)^3} \theta(\mu - \sqrt{p^2 + m_{\text{eff}}^2}) \\ &= \begin{cases} \frac{1}{\pi^2} (\sqrt{\mu^2 - m_{\text{eff}}^2})^3, & \mu > m_{\text{eff}} \\ 0, & \mu < m_{\text{eff}} \end{cases} \end{aligned} \quad (10)$$

where the subscript “i” denotes the quark of flavor i, and

<sup>2</sup> In a conventional two-flavor NJL model, the thermodynamical potential is obtained based on the mean-field approximation, see e.g. Eq. (2.46) in Ref. [50] (neglecting the contribution of the

vector interaction). The modification here can be regarded as a scheme beyond the mean-field approach, and it is hard to find a closed and easily tractable effective potential (a more detailed analysis can be found in Sec. 2 of Ref. [43]).

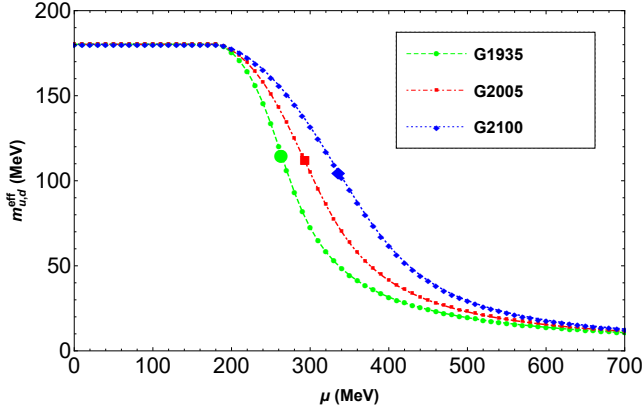


FIG. 1. The effective quark mass versus  $\mu$  at  $T = 0$ . The lines marked with G1935, G2005, and G2100 correspond to the three parameter sets in Table. I, with  $G_1 = 1.935, 2.005, 2.100$   $\text{GeV}^{-2}$ , respectively. The pseudo-critical point is also marked on each line, at  $\mu = 263, 293, 336$  MeV, respectively.

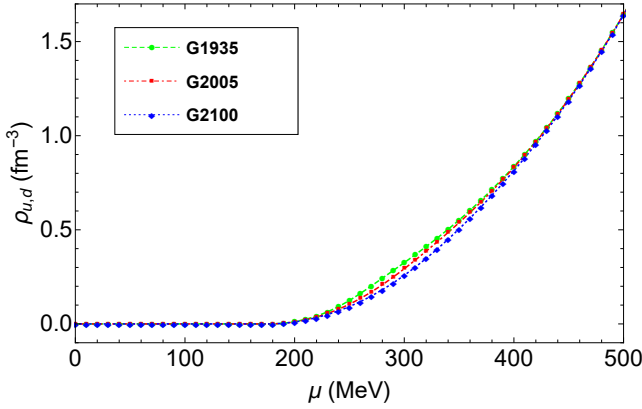


FIG. 2. The number density of  $u, d$  quarks versus  $\mu$  at  $T = 0$  for the three parameter sets in Table. I. Line styles are the same as those in Fig. 1.

the trace “tr” is calculated in the Dirac space. The effective quark mass  $m_{u,d}^{\text{eff}}$  as a function of the chemical potential at zero temperature is shown in Fig. 1. The number density  $\rho_{u,d}$  is correspondingly illustrated in Fig. 2.

From Fig. 1, we can see that for all the three parameter sets in Table. I, there is only crossover but no any chiral phase transitions as the chemical potential increases from 0 to 700 MeV. Note that the chemical potential of the pseudo-critical point is different for the three lines, as marked in Fig. 1. It can also be seen that at zero temperature and zero chemical potential, the effective quark masses are the same for the three parameter sets. This is easy to understand. Under such a condition,  $G_1 + G_2 \langle \bar{\psi}\psi \rangle$  simply reduces to  $G$ , which is exactly the coupling constant of conventional NJL model. In Fig. 2, we see that the quark densities differ only in the crossover region of  $\mu \sim (200, 400)$  MeV for the three parameter sets.

Considering the electrical neutrality of neutron stars and quark stars as well as electroweak reactions in them,

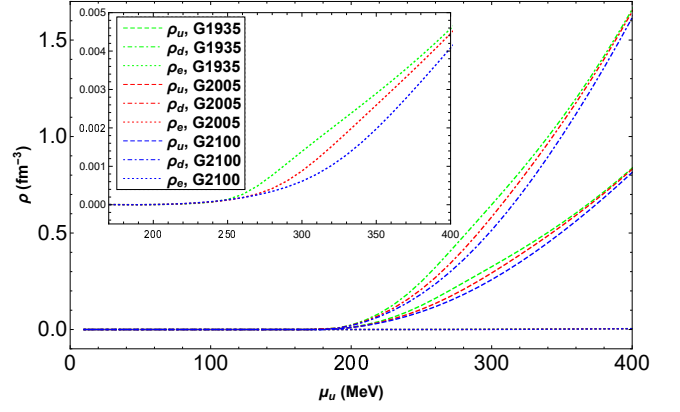


FIG. 3. The number densities of  $u, d$  quarks and electrons versus  $\mu_u$  at  $T = 0$ . The matter here is in beta equilibrium and electric charge neutrality. The parameter sets are described in Table. I. The inset shows a zoom-in of the electron densities.

we should take the beta equilibrium and electric charge neutrality conditions into account,

$$\begin{aligned} \mu_d &= \mu_u + \mu_e, \\ \frac{2}{3}\rho_u - \frac{1}{3}\rho_d - \rho_e &= 0, \end{aligned} \quad (11)$$

where the number density of electrons at zero temperature is  $\rho_e(\mu_e) = \frac{\mu_e^3}{3\pi^2}$ . The number densities of quarks and electrons incorporating these conditions are displayed in Fig. 3. We can see that in each case, the density of  $d$  quarks is larger than that of  $u$  quarks when  $\mu_u > 180$  MeV. In fact  $\rho_d$  approximately equals  $2\rho_u$ , because the electron density is much smaller. Fig. 3 also shows that as  $G_1$  increases, the constituent particle number density decreases for the same  $\mu_u$  when  $\mu_u \geq 180$  MeV. It is well known that under the beta equilibrium and electric charge neutrality conditions, the quark condensates, dynamical masses, and densities are different for  $u$  quarks and  $d$  quarks. But note that these quantities are connected with each other, and the relations between them should be considered when calculating the EOS.

By definition, the EOS of QCD for  $T = 0$  and  $\mu \neq 0$  is [59]

$$P(\mu) = P(\mu = 0) + \int_0^\mu d\mu' \rho(\mu'), \quad (12)$$

where  $P(\mu = 0)$  represents the negative vacuum pressure and is independent on the chemical potential. In general, it is treated as a phenomenological parameter which cannot be calculated model-independently. The parameter of  $P(\mu = 0)$  in QCD is equivalent to the vacuum bag constant ( $-B$ ) of the MIT bag model. Generally,  $B^{\frac{1}{4}}$  should be in a range of 100 – 200 MeV [60, 61]. More specifically, in Ref. [33] and Ref. [62], it is suggested to be 134.1 – 141.4 MeV and 166.16 – 171.06 MeV, respectively. Therefore, in this study, we will choose three represen-

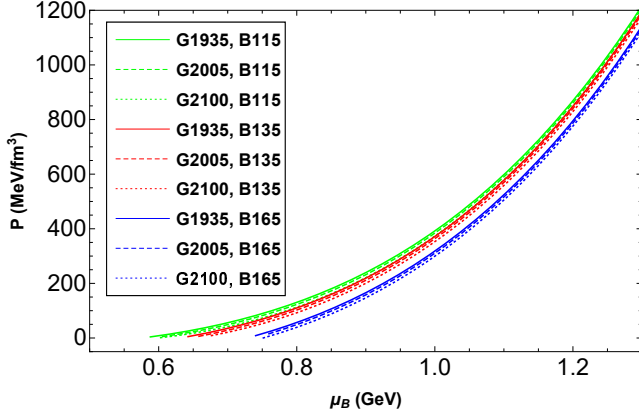


FIG. 4. The pressure as a function of the baryonic chemical potential ( $\mu_B$ ) for nine representative EOSs at  $T = 0$ . B115, B135, B165 refers to  $B^{\frac{1}{4}} = 115, 135, 165$  MeV, respectively.

tative values of  $B^{\frac{1}{4}}$  to calculate the nonstrange quark EOS, i.e.  $B^{\frac{1}{4}} = 115, 135, 165$  MeV. The results of nine representative EOSs are illustrated in Fig. 4. We see that the critical baryonic chemical potential  $\mu_{BC}$ <sup>3</sup> increases as  $B^{\frac{1}{4}}$  or  $G_1$  increases. Additionally, we see that the EOS is largely determined by the bag constant, while the parameter of  $G_1$  does not affect the EOS significantly.

The relation between the energy density and pressure is [63, 64]

$$\epsilon = -P + \sum_i \mu_i \rho_i. \quad (13)$$

To illustrate the rationality of the nine quark EOSs as well as their stiffness, we calculate the sound velocity, which is

$$\nu = \sqrt{\frac{dP}{d\epsilon}}. \quad (14)$$

The results are shown in Fig. 5. We see that the sound velocity does not exceed the conformal limit in all the cases, i.e.,  $(\nu/c)^2 \leq 1/3$ , where  $c$  is the speed of light. Usually, a larger  $G_1$  leads to a stiffer EOS. Also, note that at low energy densities, a higher vacuum pressure (i.e., a smaller  $B^{\frac{1}{4}}$ ) yields a softer EOS, but at high energy densities, the case is opposite.

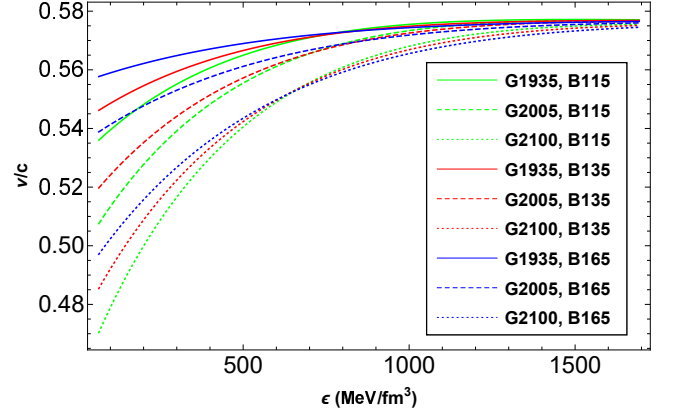


FIG. 5. The sound velocity versus energy density for the nine representative EOSs. Line styles are the same as in Fig. 4.

### III. STRUCTURE OF NONSTRANGE QUARK STARS

To study the structure of neutron stars and quark stars, we need to solve the TOV equation below,

$$\begin{aligned} \frac{dP(r)}{dr} &= -\frac{G(\epsilon + P)(M + 4\pi r^3 P)}{r(r - 2GM)}, \\ \frac{dM(r)}{dr} &= 4\pi r^2 \epsilon. \end{aligned} \quad (15)$$

Using the nine representative EOSs, we have solved the equation numerically. Our results of  $M$ - $R$  and  $M$ - $\epsilon_c$  relations are presented in Fig. 6 and Fig. 7, respectively. To constrain the EOSs, we have also plot some astronomical measurements in Fig. 6, including the largest pulsar masses (i.e.,  $2.01 \pm 0.04 M_\odot$  for PSR J0348+0432 [20], and  $2.14^{+0.10}_{-0.09} M_\odot$  for PSR J0740+6620 [21]), and the radii measured through NICER x-ray timing observations (1,  $R_{1.44M_\odot} > 10.7$  km [22]; 2,  $R_{1.4M_\odot} = 11.0^{+0.9}_{-0.6}$  km [23]; 3,  $M = 1.34^{+0.15}_{-0.16} M_\odot$  and  $R = 12.71^{+1.14}_{-1.19}$  km for PSR J0030+0451 [24]). From Fig. 6, we see that only the EOS with  $G_1 = 1.935 \text{ GeV}^{-2}$  and  $B^{\frac{1}{4}} = 115$  MeV satisfies all the above constraints, and the corresponding maximum mass of quark stars is  $2.10 M_\odot$ , with a radius of 11.69 km. When  $G_1$  is fixed, the EOS with a smaller bag constant produces a larger maximum star mass. In fig. 7, a higher maximum mass generally corresponds to a smaller central energy density.

We have also calculated the tidal deformability of quark stars. To do so, we need to solve a set of dif-

<sup>3</sup> For 2-flavor quark matter, the baryonic chemical potential is  $\mu_B = \mu_u + \mu_d$ . Note that in Fig. 4, the “critical point” refers to the condition that the pressure begins to be nonzero, not indicating any normal QCD phase transitions.



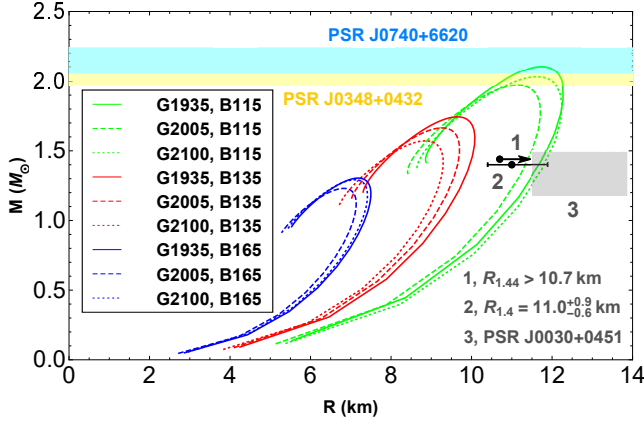


FIG. 6.  $M$ - $R$  relations for the nine representative EOSs. The mass constrains of PSR J0348+0432 [20] and PSR J0740+6620 [21], and the radius constraints from NICER x-ray timing observations [22–24] are also plot.

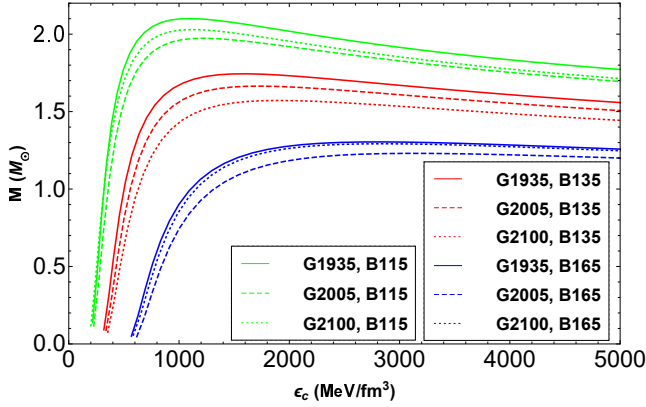


FIG. 7.  $M$ - $\epsilon_c$  relations for the nine representative EOSs.

ferential equations [65],

$$\begin{aligned} \frac{dH}{dr} &= \beta, \\ \frac{d\beta}{dr} &= 2\left(1 - 2\frac{m_r}{r}\right)^{-1} H \left\{ -2\pi[5\epsilon + 9P + f(\epsilon + P)] \right. \\ &\quad \left. + \frac{3}{r^2} + 2\left(1 - 2\frac{m_r}{r}\right)^{-1} \left(\frac{m_r}{r^2} + 4\pi r P\right)^2 \right\} \\ &\quad + \frac{2\beta}{r} \left(1 - 2\frac{m_r}{r}\right)^{-1} \left\{ \frac{m_r}{r} + 2\pi r^2(\epsilon - P) - 1 \right\}, \end{aligned} \quad (16)$$

where  $P$  and  $H(r)$  represent the pressure and the metric function, respectively, and  $f = d\epsilon/dP$ . Let us further define a parameter ( $y$ ) as  $y = R\beta(R)/H(R) - 4\pi R^3\epsilon_0/M$ , where  $\epsilon_0$  is the energy density at the surface of the star. Then the dimensionless tidal Love number  $k_2$  for  $l = 2$

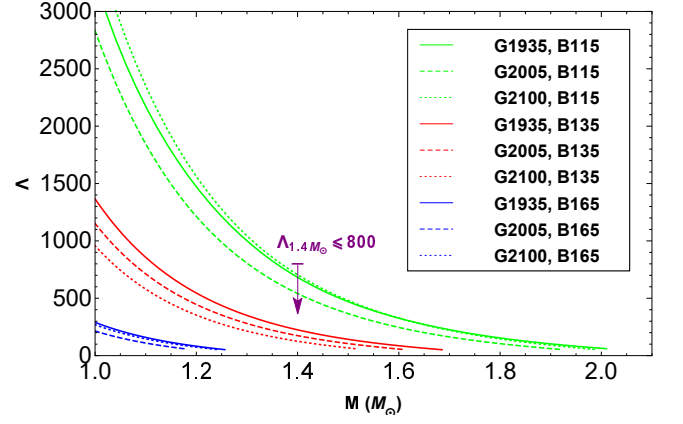


FIG. 8. Tidal deformability of nonstrange quark stars for the nine representative EOSs. The constraint of  $\Lambda(1.4M_\odot) \leq 800$  from Ref. [25] is also plot.

can be calculated as

$$\begin{aligned} k_2 &= \frac{8C^5}{5} (1 - 2C)^2 [2 + 2C(y - 1) - y] \\ &\quad \times \{ 2C[6 - 3y + 3C(5y - 8)] \\ &\quad + 4C^3[13 - 11y + C(3y - 2) + 2C^2(1 + y)] \\ &\quad + 3(1 - 2C)^2 [2 + 2C(y - 1) - y] \ln(1 - 2C) \}^{-1}, \end{aligned} \quad (17)$$

where  $C = M/R$  is the compactness of the star. According to Ref. [65], the tidal deformability is related to  $k_2$  as

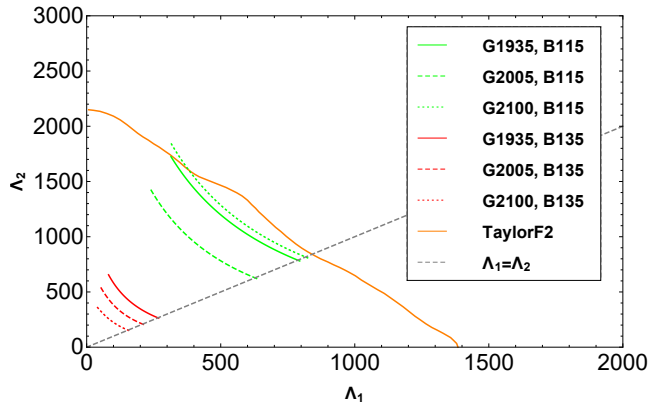
$$\Lambda = \frac{2}{3} k_2 R^5. \quad (18)$$

Note that the quark matter in quark stars is in a deconfined state. It produces a non-negative pressure at the surface. Due to the negative vacuum pressure in Eq. (12) and the negative term  $-4\pi R^3\epsilon_0/M$  in the formula of  $y$ , the quark density should be nonzero at the surface.

Our numerical results on the tidal deformability of nonstrange quark stars for the nine representative EOSs are shown in Fig. 8. We see that the tidal deformability decreases monotonously as the mass increases. EOSs with  $B^{\frac{1}{4}} = 115, 135$  MeV satisfy the constraint of  $\Lambda(1.4M_\odot) \leq 800$  derived from the observations of GW170817 for the low-spin priors [25]. Furthermore, based on the waveform model of TaylorF2, the chirp mass  $\mathcal{M} = (M_1 M_2)^{3/5} (M_1 + M_2)^{-1/5}$  is restricted to be  $1.186 \pm 0.0001 M_\odot$ , providing further constraint on companion mass of  $M_1$  and  $M_2$  for GW170817 [41]. Thus the  $\Lambda_1 - \Lambda_2$  relation of the BNS can be obtained for our nine representative EOSs, which is shown in Fig. 9. Here, the constraint from GW170817 based on the TaylorF2 waveform model [41] is also plot for a direct comparison. We see that every EOS with  $M_{\max} \geq 1.36 M_\odot$  (i.e., the EOSs with  $B^{\frac{1}{4}} = 115, 135$  MeV) fulfills the constraint except for the EOS with  $G_1 = 2.1$  GeV $^{-2}$  and  $B^{\frac{1}{4}} = 115$  MeV. In addition to that, a larger  $B^{\frac{1}{4}}$  makes the curve closer

TABLE II. Properties of nonstrange quark stars for the nine representative EOSs.

$B^{\frac{1}{4}}$ [MeV]	$G_1$ [GeV $^{-2}$ ]	$M_{\max}$ [ $M_{\odot}$ ]	$R_m$ [km]	$\epsilon_0$ [MeV/fm $^3$ ]	$\epsilon_c$ [MeV/fm $^3$ ]	$\Lambda(1.4)$ —	$R(1.4)$ [km]	$\Lambda(1.6)$ —	$R(1.6)$ [km]
115	1.935	2.10	11.69	178	1118	679	11.70	324	12.01
	2.005	1.97	11.14	188	1227	539	11.35	246	11.60
	2.100	2.03	11.62	166	1113	702	11.83	325	12.10
135	1.935	1.74	9.63	277	1612	222	9.96	83	10.08
	2.005	1.66	9.25	291	1756	176	9.65	59	9.64
	2.100	1.57	8.85	305	1909	124	9.31	—	—
165	1.935	1.30	7.17	513	2848	—	—	—	—
	2.005	1.23	6.84	555	3066	—	—	—	—
	2.100	1.29	7.09	521	2860	—	—	—	—

FIG. 9.  $\Lambda_1 - \Lambda_2$  relations for the nine representative EOSs. The observational constraint from GW170817 based on the TaylorF2 waveform model is also plot for comparison [41].

to the lower left corner of the figure.

For the sake of completeness, the properties of non-strange quark stars for the nine representative EOSs are

summarized in Table. II. The parameters listed include the mass, radius, surface and central energy densities of the heaviest star, and the tidal deformability and radius of a  $1.4 M_{\odot}$  /  $1.6 M_{\odot}$  star. From Fig. 6, Fig. 9, and Table. II, we can see that the parameter sets with  $B^{\frac{1}{4}} = 115$  MeV is good at supporting massive stars, while the EOSs with  $G_1 = 2.005$  GeV $^{-2}$  correspond to the original 2-flavor NJL model. Although the EOSs of the normal NJL model can satisfy the constraints of the tidal deformability from GW170817, they are not consistent with the mass constraint from PSR J0740+6620 and the radius constraint from PSR J0030+0451. In particular, for  $B^{\frac{1}{4}} = 115$  MeV, both increasing and decreasing the value of  $G_1$  can increase the maximum mass, but a too large or too small value of  $G_1$  makes the EOS conflict with the tidal deformability measurement of GW170817. Among the nine representative EOSs, only the one with  $B^{\frac{1}{4}} = 115$  MeV and  $G_1 = 1.935$  GeV $^{-2}$  is in agreement with all current astronomical measurements considered in this study. Based on these analyses, we argue that nonstrange quark stars might exist in the universe.

#### IV. SUMMARY AND DISCUSSION

The EOS of a modified 2-flavor NJL model with PTR is introduced to investigate the properties of nonstrange quark stars. Since the coupling constant  $G$  in the normal NJL model is an indication of the effective gluon propagator, it should not be “constant” according to the simulation of lattice QCD. The corresponding DS equation should be coupled with that of quarks by QCD in essence. Inspired by the OPE method, the coupling constant  $G$  is modified as  $G = G_1 + G_2 \langle \bar{\psi}\psi \rangle$  in this study, similar to the treatment in Refs. [7, 42–48]. The electric charge neutrality and beta equilibrium are considered in

our calculations. Nine representative EOSs are obtained for nonstrange quark stars, corresponding to different combinations of  $G_1$  and  $B$  (the bag constant) parameters. The sound velocity is calculated to illustrate the stiffness and rationality of the EOSs. It is found that the sound velocity is ubiquitously smaller than the speed of light, not exceeding the conformal limit for dense matter. It is also found that a larger  $G_1$  usually leads to a stiffer EOS. Interestingly, for the bag constant, a smaller  $B$  parameter yields a softer EOS at low densities; but at high densities, the case is opposite.

The  $M$ - $R$ ,  $M$ - $\epsilon_c$  relations and the tidal deformability of quark stars are calculated based on our new EOSs. The results are directly compared with recent astronomical

observations, including the mass measurements of PSR J0740+6620 ( $2.14^{+0.10}_{-0.09} M_{\odot}$ ) [21] and PSR J0348+0432 ( $2.01 \pm 0.04 M_{\odot}$ ) [20], the radius measurements by NICER ( $R_{1.44 M_{\odot}} > 10.7$  km [22],  $R_{1.4 M_{\odot}} = 11.0^{+0.9}_{-0.6}$  km [23],  $M = 1.34^{+0.15}_{-0.16} M_{\odot}$  and  $R = 12.71^{+1.14}_{-1.19}$  km for PSR J0030+0451 [24]), and the tidal deformability constraints from GW170817 [25, 41]. It is found that when the two key parameters are taken as  $G_1 = 1.935 \text{ GeV}^{-2}$  and  $B^{\frac{1}{4}} = 115 \text{ MeV}$ , the corresponding EOS can satisfy all the observational constraints listed above, strongly supporting the possible existence of nonstrange quark stars. In this case, the nonstrange quark star can have a maximum mass of  $2.1 M_{\odot}$ , with a radius of 11.69 km.

In the future, more and more astronomical measurements will be available, which can help better constraining the EOS of QCD. Note that only the relatively simple case of four-fermion interactions is considered here. But the method could also be extended to include more interactions, such as the 't Hooft and eight-quark interactions. To do that, we need to consider how to deal with their coupling consistently. For the normal SU(3) case, more free parameters (the current masses of u, d, s quarks, the coupling constants of four-, six-, eight-quark interactions,

and the ultraviolet cut-off) would be introduced to characterize the six- and eight-quark interactions in the NJL model. They should be determined through various laboratory experiments and astronomical observations, and should be considered in future theoretical studies.

## ACKNOWLEDGMENTS

This work is supported in part by the National Natural Science Foundation of China (under Grants No. 12005192, No. 12103047, No. 12233002, No. 11873030, No. 12041306, No. 12147103, and No. U1938201), the Project funded by China Postdoctoral Science Foundation (2020M672255, 2020TQ0287), National SKA Program of China No. 2020SKA0120300, the National Key R&D Program of China (2021YFA0718500), the science research grants from the China Manned Space Project with NO. CMS-CSST-2021-B11, the Natural Science Foundation of Henan Province of China (212300410290), the start-up funding from Zhengzhou University, and the High-level Talent Fund of Henan University of Technology (Grant No. 31401242).

- 
- [1] N. Itoh, *Prog. Theor. Phys.* **44**, 291 (1970).
  - [2] H. Terazawa, Tokyo University Report, page INS336 (1979).
  - [3] A. R. Bodmer, *Phys. Rev. D* **4**, 1601 (1971).
  - [4] E. Witten, *Phys. Rev. D* **30**, 272 (1984).
  - [5] E. Farhi and R. L. Jaffe, *Phys. Rev. D* **30**, 2379 (1984).
  - [6] C.-M. Li, J.-L. Zhang, T. Zhao, Y.-P. Zhao, and H.-S. Zong, *Phys. Rev. D* **95**, 056018 (2017).
  - [7] C.-M. Li, J.-L. Zhang, Y. Yan, Y.-F. Huang, and H.-S. Zong, *Phys. Rev. D* **97**, 103013 (2018).
  - [8] B.-L. Li, Z.-F. Cui, Z.-H. Yu, Y. Yan, S. An, and H.-S. Zong, *Phys. Rev. D* **99**, 043001 (2019).
  - [9] C.-M. Li, S.-Y. Zuo, Y. Yan, Y.-P. Zhao, F. Wang, Y.-F. Huang, and H.-S. Zong, *Phys. Rev. D* **101**, 063023 (2020).
  - [10] B.-L. Li, Y. Yan, and J.-L. Ping, *The European Physical Journal C* **81**, 1 (2021).
  - [11] J. Sedaghat, S. Zebarjad, G. Bordbar, and B. Eslam Panah, *Phys. Lett. B* **829**, 137032 (2022).
  - [12] J. Geng, B. Li, and Y. Huang, *Innovation* **2**, 100152 (2021).
  - [13] B. Holdom, J. Ren, and C. Zhang, *Phys. Rev. Lett.* **120**, 222001 (2018).
  - [14] Q. Wang, C. Shi, and H.-S. Zong, *Phys. Rev. D* **100**, 123003 (2019).
  - [15] T. Zhao, W. Zheng, F. Wang, C.-M. Li, Y. Yan, Y.-F. Huang, and H.-S. Zong, *Phys. Rev. D* **100**, 043018 (2019).
  - [16] C. Zhang, *Phys. Rev. D* **101**, 043003 (2020).
  - [17] J. Ren and C. Zhang, *Phys. Rev. D* **102**, 083003 (2020).
  - [18] C. Zhang and R. B. Mann, *Phys. Rev. D* **103**, 063018 (2021).
  - [19] W.-L. Yuan, A. Li, Z. Miao, B. Zuo, and Z. Bai, *Phys. Rev. D* **105**, 123004 (2022).
  - [20] J. Antoniadis, P. C. C. Freire, N. Wex, T. M. Tauris, R. S. Lynch, M. H. van Kerkwijk, M. Kramer, C. Bassa, V. S. Dhillon, T. Driebe, J. W. T. Hessels, V. M. Kaspi, V. I. Kondratiev, N. Langer, T. R. Marsh, M. A. McLaughlin, T. T. Pennucci, S. M. Ransom, I. H. Stairs, J. van Leeuwen, J. P. W. Verbiest, and D. G. Whelan, *Science* **340**, 1233232 (2013).
  - [21] H. T. Cromartie, E. Fonseca, S. M. Ransom, P. B. Demorest, Z. Arzoumanian, H. Blumer, P. R. Brook, M. E. DeCesar, T. Dolch, J. A. Ellis, *et al.*, *Nat. Astron.* **4**, 72 (2020).
  - [22] S. Bogdanov, S. Guillot, P. S. Ray, M. T. Wolff, D. Chakrabarty, W. C. Ho, M. Kerr, F. K. Lamb, A. Lommen, R. M. Ludlam, *et al.*, *Astrophys. J. Lett.* **887**, L25 (2019).
  - [23] C. D. Capano, I. Tews, S. M. Brown, B. Margalit, S. De, S. Kumar, D. A. Brown, B. Krishnan, and S. Reddy, *Nat. Astron.* **4**, 625 (2020).
  - [24] T. E. Riley, A. L. Watts, S. Bogdanov, P. S. Ray, R. M. Ludlam, S. Guillot, Z. Arzoumanian, C. L. Baker, A. V. Bilous, D. Chakrabarty, *et al.*, *Astrophys. J. Lett.* **887**, L21 (2019).
  - [25] B. P. Abbott and et al. (LIGO Scientific Collaboration and Virgo Collaboration), *Phys. Rev. Lett.* **119**, 161101 (2017).
  - [26] B. P. Abbott and et al. (LIGO Scientific Collaboration and Virgo Collaboration), *Astrophys. J. Lett.* **848**, L12 (2017).
  - [27] E. Annala, T. Gorda, A. Kurkela, and A. Vuorinen, *Phys. Rev. Lett.* **120**, 172703 (2018).
  - [28] F. J. Fattoyev, J. Piekarewicz, and C. J. Horowitz, *Phys. Rev. Lett.* **120**, 172702 (2018).
  - [29] B. Margalit and B. D. Metzger, *Astrophys. J. Lett.* **850**, L19 (2017).



- [30] A. Bauswein, O. Just, H.-T. Janka, and N. Stergioulas, *Astrophys. J. Lett.* **850**, L34 (2017).
- [31] V. Paschalidis, K. Yagi, D. Alvarez-Castillo, D. B. Blaschke, and A. Sedrakian, *Phys. Rev. D* **97**, 084038 (2018).
- [32] M. Shibata, S. Fujibayashi, K. Hotokezaka, K. Kiuchi, K. Kyutoku, Y. Sekiguchi, and M. Tanaka, *Phys. Rev. D* **96**, 123012 (2017).
- [33] E.-P. Zhou, X. Zhou, and A. Li, *Phys. Rev. D* **97**, 083015 (2018).
- [34] M. Ruiz, S. L. Shapiro, and A. Tsokaros, *Phys. Rev. D* **97**, 021501(R) (2018).
- [35] D. Radice, A. Perego, F. Zappa, and S. Bernuzzi, *Astrophys. J. Lett.* **852**, L29 (2018).
- [36] L. Rezzolla, E. R. Most, and L. R. Weih, *Astrophys. J. Lett.* **852**, L25 (2018).
- [37] R. Nandi and P. Char, *Astrophys. J* **857**, 12 (2018).
- [38] Z.-Y. Zhu, E.-P. Zhou, and A. Li, *Astrophys. J* **862**, 98 (2018), [arXiv:1802.05510](#).
- [39] S. Ai, H. Gao, Z.-G. Dai, X.-F. Wu, A. Li, B. Zhang, and M.-Z. Li, *Astrophys. J* **860**, 57 (2018), [arXiv:1802.00571](#).
- [40] Y.-L. Ma, H. K. Lee, W.-G. Paeng, and M. Rho, *Sci. China Phys. Mech.* **62**, 1 (2019).
- [41] B. P. Abbott and et al. (LIGO Scientific Collaboration and Virgo Collaboration), *Phys. Rev. X* **9**, 011001 (2019).
- [42] Y. Jiang, H. Gong, W.-M. Sun, and H.-S. Zong, *Phys. Rev. D* **85**, 034031 (2012).
- [43] Z.-F. Cui, C. Shi, Y.-H. Xia, Y. Jiang, and H.-S. Zong, *Eur. Phys. J. C* **73**, 2612 (2013).
- [44] Z.-F. Cui, C. Shi, W.-M. Sun, Y.-L. Wang, and H.-S. Zong, *Eur. Phys. J. C* **74**, 2782 (2014).
- [45] C. Shi, Y.-L. Du, S.-S. Xu, X.-J. Liu, and H.-S. Zong, *Phys. Rev. D* **93**, 036006 (2016).
- [46] Q.-W. Wang, Z.-F. Cui, and H.-S. Zong, *Phys. Rev. D* **94**, 096003 (2016).
- [47] Z.-Y. Fan, W.-K. Fan, Q.-W. Wang, and H.-S. Zong, *Mod. Phys. Lett. A* **32**, 1750107 (2017).
- [48] W. Fan, X. Luo, and H. Zong, *Chin. Phys. C* **43**, 054109 (2019).
- [49] S. P. Klevansky, *Rev. Mod. Phys.* **64**, 649 (1992).
- [50] M. Buballa, *Phys. Rep.* **407**, 205 (2005).
- [51] Z.-F. Cui, S.-S. Xu, B.-L. Li, A. Sun, J.-B. Zhang, and H.-S. Zong, *Eur. Phys. J. C* **78**, 770 (2018).
- [52] S.-S. Xu, Z.-F. Cui, A. Sun, and H.-S. Zong, *J. Phys. G: Nucl. Part. Phys.* **45**, 105001 (2018).
- [53] C.-M. Li, P.-L. Yin, and H.-S. Zong, *Phys. Rev. D* **99**, 076006 (2019).
- [54] L. Reinders, H. Rubinstein, and S. Yazaki, *Phys. Rep.* **127**, 1 (1985).
- [55] T. G. Steele, *Z. Phys. C* **42**, 499 (1989).
- [56] P. Pascual and R. Tarrach, *QCD: Renormalization for the Practitioner* (Springer, 1984).
- [57] Particle Data Group, P. Zyla, R. Barnett, and et al., *Prog. Theor. Exp. Phys.* **2020**, 1 (2020).
- [58] H.-S. Zong, L. Chang, F.-Y. Hou, W.-M. Sun, and Y.-X. Liu, *Phys. Rev. C* **71**, 015205 (2005).
- [59] H.-S. Zong and W.-M. Sun, *Int. J. Mod. Phys. A* **23**, 3591 (2008).
- [60] D. Lu, K. Tsushima, A. Thomas, A. Williams, and K. Saito, *Nucl. Phys. A* **634**, 443 (1998).
- [61] G. Song, W. Enke, and L. Jiarong, *Phys. Rev. D* **46**, 3211 (1992).
- [62] C.-M. Li, Y. Yan, J.-J. Geng, Y.-F. Huang, and H.-S. Zong, *Phys. Rev. D* **98**, 083013 (2018).
- [63] Y. Yan, J. Cao, X.-L. Luo, W.-M. Sun, and H.-S. Zong, *Phys. Rev. D* **86**, 114028 (2012).
- [64] O. G. Benvenuto and G. Lugones, *Phys. Rev. D* **51**, 1989 (1995).
- [65] T. Hinderer, B. D. Lackey, R. N. Lang, and J. S. Read, *Phys. Rev. D* **81**, 123016 (2010).